JOURNAL OF THERMOPHYSICS AND HEAT TRANSFER
Vol. 8, No. 3, July–Sept. 1994

Experimental and Analytical Investigation of a Capillary Pumped Loop

J. T. Dickey* and G. P. Peterson†
Texas A&M University, College Station, Texas 77843

An experimental investigation was conducted on a relatively new and unique type of capillary pumped loop (CPL) at various power inputs and adverse tilts in order to verify the operational parameters and measure the performance limits. A concurrently developed computer model was compared with the experimental data to determine the accuracy of the model and verify the predicted trends. The model shows good agreement with the experimental data and indicates that the overall transport capacity of this design is significantly greater than what would normally be expected in conventional heat pipes. The steady-state temperature variations are presented as a function of input power and adverse tilt, along with the transient response characteristics of the CPL. Also, a comparison is made between data obtained by the authors and that supplied by the manufacturer.

Nomenclature

D = diameter
D_h = hydraulic diameter
h = coefficient of convection
h_{fg} = latent heat of vaporization
K_w = wick permeability
k = thermal conductivity
L = length
$\dot{m}$ = mass flow rate
Re = Reynolds number
S = shape factor
T = temperature
x = axial distance
x^+ = distance parameter
ΔP_c = capillary pressure
ΔP_f = fluid pressure losses
ΔP_g = hydrostatic pressure losses
ΔP_l = liquid pressure losses
ΔP_t = pressure due to temperature difference
ΔP_w = pressure losses in the wick
λ = latent heat of vaporization
μ = viscosity

Subscripts
c = condenser
e = evaporator
i = inner
l = liquid
o = outer
s = saturation
t = total
v = vapor
w = wall

Introduction

CAPILLARY pumped loops (CPL) are two-phase thermal control systems that can satisfy the increasingly rigorous requirements projected for future spacecraft. For this reason, these devices have been selected as the baseline design for the thermal control system of the Earth Observing System (EOS).[1] CPLs offer large heat load carrying capacities with substantial wicking heights in gravity environments, particularly when compared to conventional heat pipes. Other advantages of CPLs are the local position of the wick in the evaporation zone, which provides low wick pressure losses with high capillary pumping and the capability of operating as a thermal diode.

As is the case for conventional heat pipes, the high effective thermal conductivity of CPLs results from the vaporization and condensation of the working fluid. A major difference is that in a CPL, the liquid and vapor flows are separated, thereby allowing the vapor to be slightly superheated and the liquid to be subcooled. Under these conditions, the overall transport capacity of the loop is increased due to sensible heating. For this reason, determination of how the input energy affects the operating temperature of the working fluid in both the liquid and vapor states plays a key role in establishing the heat transport characteristics and operational limitations of these devices.

Initial investigations of CPLs began in the late fifties with the capillary pumped vapor generator work of Laub[2] and McGinness.[3] In the mid-sixties, a feasibility study was conducted by Stenger[4] at the Lewis Research Center. In this investigation, two CPLs capable of transporting more than 800 W over a distance of 50 ft were evaluated to determine the general operating attributes. Over the next 20 yr very little research was performed to quantify the operational parameters of these devices. Starting in the mid-eighties, however, a resurgence in CPL investigations shed new light on the advantages, commercial potential, and problems associated with these devices.

The primary focus of the current investigation was to analyze, model, and test a two-phase heat transfer device similar to conventional CPLs. The analysis and tests were conducted for a range of operating temperatures, power inputs, and adverse tilt angles. To separate the effects of these variables, the initial tests were conducted in a horizontal orientation, whereas the condenser temperature and power input were varied. In the second phase of the investigation, the tilt angle, power input, and condenser temperature were all varied sequentially to evaluate the effects of each of these three parameters. In the final phase, the transient response characteristics of the loop were evaluated.

A description of the basic operating principles of the CPL used in the current investigation were first presented by Maidanik.[5] The present investigation utilized a Model LA-ITF-07 test article provided by the Lavochkin Scientific and

Received July 7, 1993; revision received Jan. 20, 1994; accepted for publication Jan. 20, 1994.

*Research Assistant, Department of Mechanical Engineering.
†Tenneco Professor and Head, Department of Mechanical Engineering. Associate Fellow AIAA.

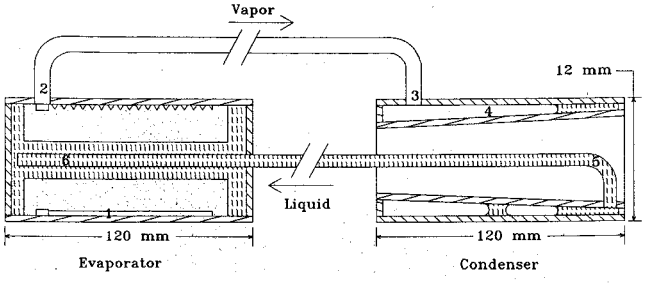

Fig. 1 Capillary pumped loop.

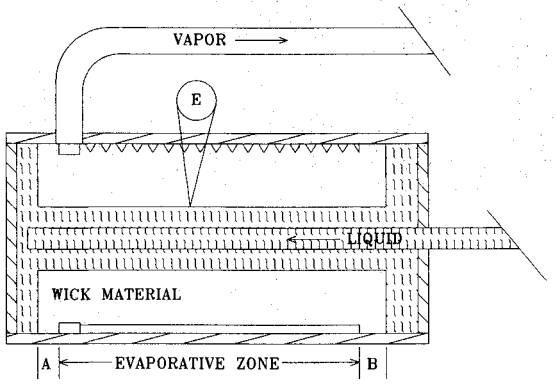

Fig. 2 Evaporator schematic.

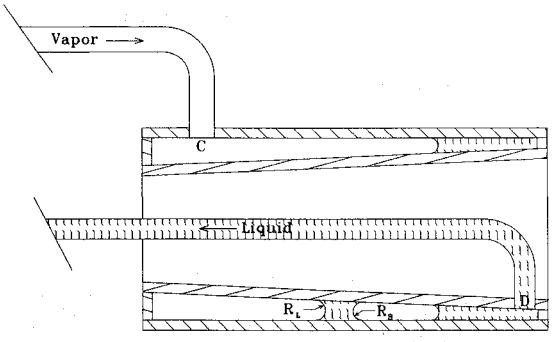

Fig. 3 Condenser schematic.

Production Association, with ammonia as the working fluid. Figure 1 illustrates an internal schematic of the CPL test article. As shown, the condenser and evaporator are approximately 120 mm long, have an o.d. of 12 mm, and are housed in aluminum saddles, 50 mm wide, 120 mm long, and 19 mm thick, and are separated by two stainless steel tubes, one for vapor flow and one for liquid return. The vapor tube has an o.d. of 4 mm and an i.d. of 3 mm, whereas the liquid line has i.d. and o.d. of 2 and 3 mm, respectively. The inherent flexibility of the tubing allows the relative position to be varied with a maximum separation distance of approximately 3 m.

The evaporator, shown in Fig. 2, consists of a cylindrical-powdered metal wick, inserted into a stainless steel housing. The wick is constructed from a sintered nickel powder with an average pore radius between 1–1.5 μ, and a porosity of 70%. The wick is sealed circumferentially to the housing at points "A" and "B," preventing the flow of vapor between the housing and wicking structure. In the evaporator, liquid which was carried to the evaporative zone via the wick material, undergoes a phase change as power is applied to the evaporator. The pressure generated by the small capillary radius of the porous wicking structure acts as a deterrent to prevent vapor from passing through the wicking structure and filling the liquid region of the evaporator with vapor, which would cause the device to fail. The increased pressure resulting from liquid changing to vapor in the evaporator, then forces the vapor to flow to the condenser shown in Fig. 3, through 4-mm stainless steel tubing.

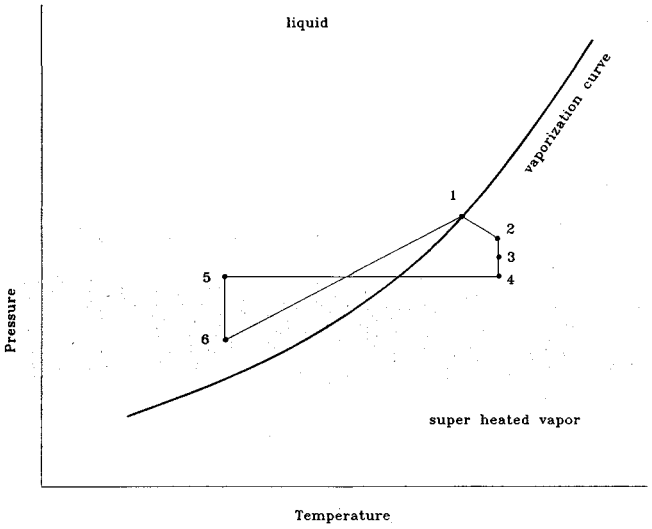

Fig. 4 Pressure temperature relationship for the CPL locations.

In the condenser region, the vapor enters at point "C" and condenses on the outer walls, forming a liquid slug. Because the liquid condensate region is tapered, once the condensate contacts the opposite wall, the liquid bridges and forms two radii of curvature R_L and R_S. Utilizing the capillary pressure drop across the interface as described by the Young-LaPlace equation

$$\Delta P_c = (2\sigma/r_c) \tag{1}$$

and realizing that $R_L > R_S$, it can be shown that in the absence of gravitational body forces the liquid will be induced to flow in the direction of the smaller radius, forming a liquid reservoir at the narrow end of the tapered chamber. The liquid exits the condenser at point "D" through the 3-mm stainless steel tubing, due to a combination of the high vapor pressure generated in the evaporator and the high capillary pressure difference supported in the evaporator wick structure.

Figure 4 illustrates the thermodynamic cycle upon which the CPL investigated here operates, and is similar to one developed by Maidanik et al.[6] The corresponding state locations are illustrated in Fig. 1. (When viewing Fig. 1 it is important to remember that the third axis of a P-T diagram is the specific volume and the saturation line is actually a surface which varies as the specific volume changes.) State 1 represents the conditions at the evaporator surface. As thermal energy is added to the working fluid, the liquid is vaporized and travels circumferentially to the evaporator exit, where the vapor (indicated by point 2) is in a slightly superheated condition due to a small decrease in the pressure and an increase in temperature caused by contact with the evaporator wall, which is at a temperature greater than T_{sat}. Between locations 2 and 3 the vapor undergoes a constant temperature pressure decrease caused by the frictional pressure drop occurring in the vapor tube. Ideally, the conditions in the condenser, i.e., state 3, are those of a saturated vapor, however, in reality the vapor may still be slightly superheated. Between states 3 and 4, vapor is condensed and drawn into the liquid reservoir by the capillary pressure generated when a condensate droplet bridges the tapered gap. The time necessary for fluid to travel through the condenser and exit, state 5, allows the liquid to be slightly subcooled. Between states 5 and 6, subcooled liquid is drawn through the liquid tube at a constant temperature and decreased pressure due to frictional losses in the liquid line. This liquid motion is the result of a combination of the capillary pumping and the difference in pressure across the wick structure. The pressure difference due to the temperature gradient across the wick can be determined utilizing the Clausius-Clapeyron equation:

$$\Delta P_t = (h_{fg} P_v \Delta T / R T_v^2) \tag{2}$$

As liquid is drawn back to the evaporator surface, state 1, through the wick material by the capillary structure, the liquid undergoes both a temperature and pressure increase. At this point the cycle begins anew.

Determination of the operating pressure loss occurring in various types of capillary structures and porous media has been the subject of extensive investigation.[7,8] For fluid flow in smooth tubing the pressure loss ΔP_f is characterized by a friction factor f. If the flow is laminar then this value can be approximated as $f = 64/Re$, and the overall pressure drop expressed as

$$\Delta P_f = (64/Re)(L/D)(\bar{V}^2/2) \tag{3}$$

In general, the pressure losses in the capillary wicking structure can be characterized by the liquid viscosity and wick permeability, thus

$$\Delta P_{\text{wick}} = \left(\frac{\mu_l Q}{2\pi\lambda K_{\text{wick}} L_{\text{wick}}}\right)\left(\frac{D_o}{D_i}\right) \tag{4}$$

The gravity pressure losses are simply the result of hydrostatic pressure and, with the exception of variations in the density, are not temperature-dependent:

$$\Delta P_g = \rho g h \tag{5}$$

Utilizing these expressions, a pressure balance across the meniscus indicates that the pressure loss associated with the bulk fluid motion must be less than or equal to the driving pressure forces or

$$\Delta P_c + \Delta P_l \geq \Delta P_{\text{wick}} + \Delta P_f + \Delta P_g \tag{6}$$

When these conditions are met, the system will operate, otherwise, evaporator dry-out and total failure will occur.

Experimental Test Facility

Figure 5 depicts the placement of 15 thermocouples utilized during the test procedure. Data from the thermocouple and two multimeters, employed to determine the input power, were obtained using a computerized data acquisition system. Multiple measurements from the same zones (i.e., the evaporator and condenser regions and the liquid and vapor tubes) were averaged to produce a time and spatially averaged temperature for each power input level. Data were averaged over an 8-min time interval to reduce the effects of transient slug flow in the condenser. Errors associated with the thermocouple reads are on the order of 0.1°C, and those of the multimeters have reported error values of no more than 0.0003% for ac current.

The experimental data obtained included the condenser temperature, power input, and the elevation difference between the evaporator and the condenser. Heat removal was provided at the condenser by placing a Lexan® cooling chamber, connected to a constant temperature bath of ethylene glycol, on either side. The condenser temperature was maintained at a predetermined value by modifying the set point of the constant temperature bath. At low condenser temperatures and high power inputs, a cryogenic coolant (liquid nitrogen) was necessary to maintain the required condenser temperature. Power was supplied to the evaporator by a variable voltage source connected to a strip heater wrapped around the evaporator. The heater was coated with a thermally conductive grease to ensure good thermal contact. Power increments of 10 W were utilized to increase the thermal input power to the evaporator for constant condenser temperatures of 0°C. For a condenser temperature of 30°C, the power was increased in 20-W increments. The condenser, vapor, and liquid lines were encased in fiberglass insulation to reduce the heat loss in the transport sections. Due to the high temperature requirements, the evaporator was wrapped in a ceramic insulation.

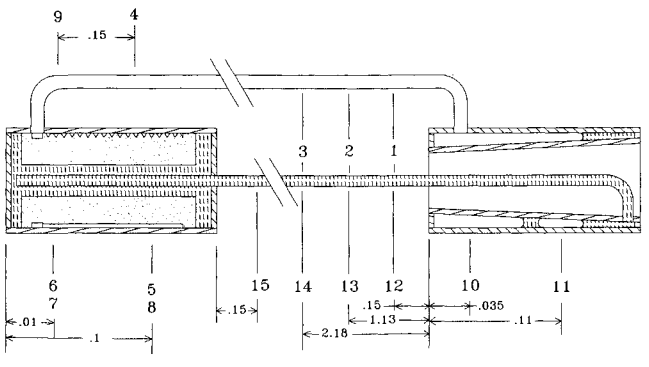

Fig. 5 Placement of thermocouples (all dimensions are in meters).

Operation of the CPL was limited to a temperature of less than 100°C in the liquid and vapor transport tubes to prevent overpressurization and rupture of the containment vessel. Determination of the heat loss at the evaporator was resolved by a pair of thermocouples placed just inside and outside the insulation at the evaporator. Knowing this temperature difference and thermal conductivity of the insulation, the energy losses occurring at the evaporator could be estimated and the input thermal power corrected. To accommodate variations in tilt angle, the unit was mounted on a 25- × 150-mm test fixture approximately 4 m long. An elevation control system was attached to the evaporator end to allow the test fixture to be raised or lowered to the desired elevation.

Analytical Model

An energy balance at the evaporator and condenser regions can be expressed as

$$Q_t = Q_{h_{fg}} + Q_{c_p\Delta T,\text{liq}} + Q_{c_p\Delta T,\text{vapor}} \tag{7}$$

If the energy required for a temperature change in the vapor due to sensible heating is assumed to be small compared to the energy required for phase change and sensible heating of the liquid, Eq. (4) reduces to

$$Q_t = Q_{h_{fg}} + Q_{c_p,\Delta T} \tag{8}$$

Upon examination of the liquid temperature change in the condenser section, the sensible heating of the working fluid can be expressed as

$$Q_{c_p,\Delta T} = \dot{m}c_p(T_s - T_l) \tag{9}$$

$$Q_{c_p,\Delta T} = A_c h_c \left\{T_{w,c} - \left[\frac{(T_s + T_l)}{2}\right]\right\} \tag{10}$$

Combining these two equations allows an expression for T_l to be written as

$$T_l = \frac{A_c h_c T_{w,c} - T_s[(A_c h_c/2) + \dot{m}c_{p,l}]}{(A_c h_c/2) - \dot{m}c_p} \tag{11}$$

In addition, an expression for the total energy in the evaporator $Q_{t,e}$ may be written as

$$Q_{t,e} = \dot{m}h_{fg} + \dot{m}c_p(T_s - T_l) \tag{12}$$

Similarly, the total energy in the condenser $Q_{t,c}$ can be expressed as

$$Q_{t,c} = \dot{m}h_{fg} + A_c h_c(T_l - T_{w,c}) \tag{13}$$

Solving for T_l in the above equation and substituting into Eq. (9) yields a second-order equation with respect to the mass

flow rate. Rearranging this expression results in a quadratic expression of the form

$$0 = \dot{m}^2(c_p h_{fg}/A_c h_c) + \dot{m}[h_{fg} + c_p T_s - (c_p Q_{\text{total}}/A_c h_c) - c_p T_{w,c}] - Q_{\text{total}} \quad (14)$$

where the values for $T_{w,c}$, h_{fg}, c_p, A_c, and h_c can all be either measured or estimated. The area of the condenser A_c can be approximated with knowledge of the following properties: liquid and vapor density at the specified temperatures, initial charge, and total internal volume of the CPL. The condenser wall temperature $T_{w,c}$ is a strong function of the geometry in which the condenser is housed. By using a finite element model with the appropriate boundary conditions, or utilizing a shape factor analysis, the wall temperature of the condenser may also be determined. Both approaches have been presented previously.[9]

The Nusselt numbers and influence coefficients for the circular tube annulus family can be determined based on x^+ and the condenser geometry,[10] where

$$x^+ = [2(x/D_h)/RePr] \quad (15)$$

Then, from the definition of the Nusselt number, $Nu = h_c D_h/k_l$, the coefficient of convection can be estimated.

Solutions to this expression can be obtained utilizing an iterative method, Eqs. (2) and (8), the positive root of the second-order equation, and updated values of the geometric and thermodynamic properties. This allows the values of the bulk temperatures of the liquid and vapor and the mass flow rate to be determined for the CPL in a horizontal orientation.

When the CPL is placed with the evaporator above the condenser (adverse tilt), the internal pressure must include both the pressure resulting from the temperature increase and the hydrostatic pressure. For small tilt angles, an estimate of the vapor pressure can be obtained by combining the hydrostatic pressure caused by the elevation difference and the pressure generated at the specified input power in a horizontal position, or

$$P_{s,2} = P_{s,1} + \rho g h \quad (16)$$

where the subscripts 1 and 2 represent horizontal and some specified adverse tilt orientation, respectively. From this pressure the thermodynamic properties can be determined.

Finally, the liquid temperature can be expressed as shown in Eq. (9), and T_l may be written as

$$T_l = T_{s,2} - [(Q - \dot{m}h_{fg})/\dot{m}c_{p,l}] \quad (17)$$

Again, the solution requires the use of an iterative method, Eqs. (11) and (13), and updated thermodynamic and geometric properties at each iteration. Utilizing this procedure, solutions for the mass flow rate, average liquid temperature, and average vapor temperature can be obtained.

Results and Discussion

As discussed previously, the wick serves three primary functions: 1) to act as a vapor barrier preventing reverse vapor flow, 2) to act as a capillary wicking structure to draw fluid from the condenser to the evaporator, and 3) to act as a thermal barrier to reduce the heat transfer from the outer region of the wick, which is at T_s to the inner region of the wick where subcooled liquid exists. The first two of these have been examined earlier. The third function is most easily explained by examining the point where liquid just begins to enter the wick.

Referencing Fig. 2 and assuming the CPL is in an adverse vertical alignment, at point "E" the effect of the gravity pressure loss is most pronounced since it is the highest point in the CPL cycle. Also, the temperature of the liquid at point C is elevated due to conduction through the wick. The rate of conduction is dependent on the wick structure, wick material, working fluid, saturation temperature, and the mass flow rate through the wick. Thus, a low liquid pressure and high vapor pressure occur in the liquid at point E, the inner surface of the wick. In order to avoid boiling, the pressure of the entire CPL system must be increased such that the hydraulic pressure loss is balanced by the pressure gradient across the wick [Eq. (2)]. A wick material of low conductivity, such as ceramic, could be utilized to increase the temperature difference, thereby, increasing the adverse difference in elevation between condenser and evaporator, at which this type of device could operate.

In the test apparatus, dry-out of the wick becomes prevalent with increasing elevation at low power inputs due to conduction through the wick material, Fig. 6 illustrates this situation. Initially, the system pressure is high to accommodate a low mass flow rate through the wick, i.e., a small temperature difference across the wick. Then, as more power is applied, the mass flow rate increases and the temperature difference across the wick becomes larger. This allows the system temperature/pressure to decrease initially, then rise as more power is transported by the CPL.

Figure 7 compares the measured and predicted temperature of the liquid and vapor in the transport sections, for an input power of 130 W as a function of adverse tilt. As illustrated, the correlation between the experimental and theoretical results is quite good. The basic operating characteristics for the vapor indicate a linearly constant region followed by an exponential increase. The increase can be attributed to the pressure necessary to maintain the working fluid in a liquid state at the evaporator. At low adverse tilt angles the subcooling of the liquid is sufficient to prevent vaporization of liquid at the internal surface of the wick. As the tilt angle increases, the subcooling of the liquid is no longer sufficient to prevent boiling. The shape is a function of the working fluid properties

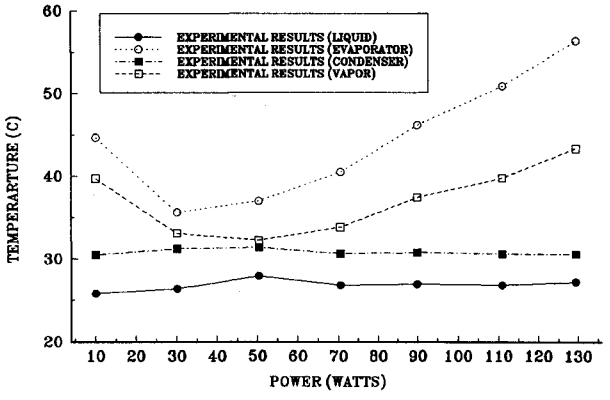

Fig. 6 Adverse height of 0.58 m.

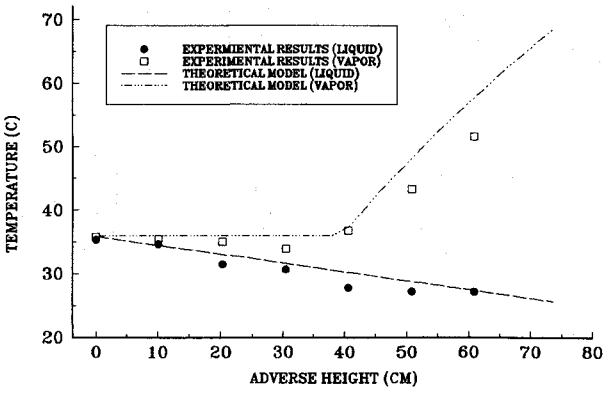

Fig. 7 Comparison of experimental and theoretical results.

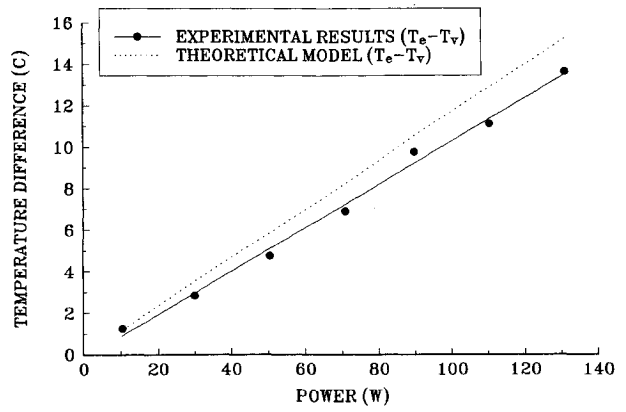

Fig. 8 Evaporator and vapor temperature difference.

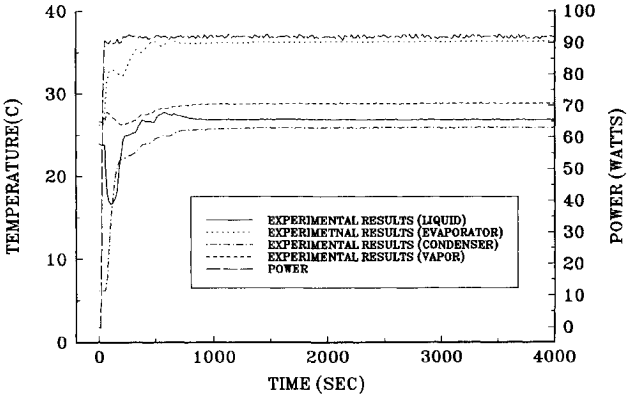

Fig. 9 Transient response.

and the mass flow rate, which are nonlinear with temperature and power input, respectively.

The linear decrease in liquid line temperature can be explained by examining the conduction equation utilizing a shape factor or

$$Q = kS(T_{\text{outer}} - T_{\text{inner}}) \tag{18}$$

where T_{outer} and T_{inner} are the outside and center temperatures of the aluminum saddle, respectively. The thermal conductivity of the aluminum saddles and shape factor can be taken as constant values. Although the averaged temperature of the condenser can also be considered a constant, the coolant bath temperature actually decreases as the power input increases. The deviation of data from the predicted values can be partially attributed to thermocouple location on the condenser.

To determine the temperature characteristics of the evaporator with respect to the power input, another shape factor, based on the construction of a flux plot, was utilized. This method resulted in a S of 0.0762 m. This value takes into account that power is applied to the evaporator over a length of 0.019 m (0.75 in.) (the width of the strip heater). Figure 8 compares the difference in temperature between the vapor and the evaporator wall obtained by the experimental tests and analytical model. As illustrated, the agreement is quite good. If the predicted temperature difference is added to the vapor model, then an estimate of the evaporator temperature can be obtained. The deviation between the analytical predictions and experimental results is due in part to conduction within the aluminum saddle.

Transient startup responses are shown in Fig. 9 for a power input of 90 W. Time constants for this case are on the order of 130, 250, 350, and 600 s for the condenser, evaporator, vapor line, and liquid line, respectively.

Also of interest to the designer of a CPL system is the apparent thermal resistance, defined as

$$R_{\text{eff}} = (\Delta T/Q) \tag{19}$$

Where ΔT is the difference in thermocouple reading between the evaporator and condenser. Figures 10 and 11 show the apparent thermal resistance as a function of power input and adverse height difference, respectively. As shown in the figures, the effective thermal resistance is quite low, approximately 0.15°C/W over much of the range tested. Noticeable exceptions arise at low power inputs where a low mass flow rate results in a small temperature difference across the wick material.

The reported temperature response of the CPL evaporator wall temperature and experimental results for all four zones, utilizing a constant bath temperature of 0°C, are shown in Fig. 12. The extracted evaporator wall value represents the measured evaporator temperature minus the difference in temperature as determined by Eq. (18) for the evaporator (Fig. 8). For low mass flow rates (i.e., low power inputs), the wall and vapor temperatures are approximately equal due to low vapor velocity through the evaporator. As the power increases, so does the vapor velocity, thereby increasing the temperature difference between the vapor and evaporator

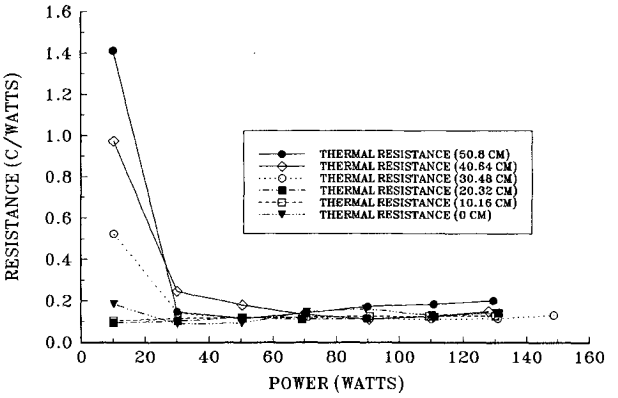

Fig. 10 Effective thermal resistance as a function of power.

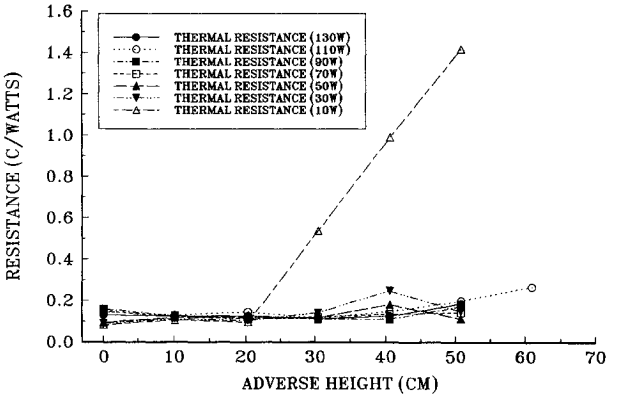

Fig. 11 Effective thermal resistance as a function of height.

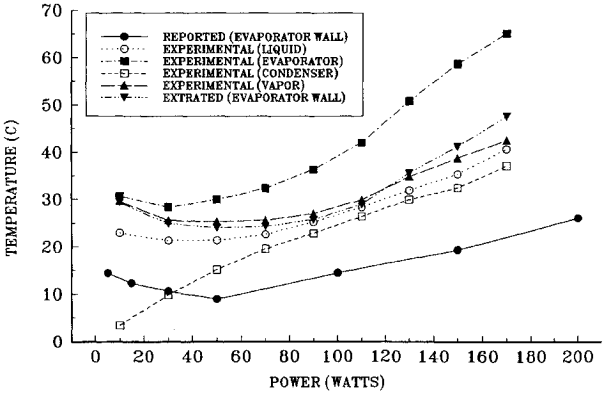

Fig. 12 Measured and reported performance.

wall due to the decrease in time it requires for vapor to flow out of the evaporator. The trend of the extracted evaporator wall temperatures shows good agreement with the reported values provided by the Lavochkin Scientific and Production Association.[6] The variation in results may be attributable to a difference in coolant bath velocity, which was not reported in Ref. 6. A low coolant velocity passing over the condenser will have a smaller convection coefficient than a higher velocity coolant passing over the same condenser geometry. Thus, the temperature of the entire CPL will be increased as a result of low coolant velocity. Also, it is not clear what type, or even if, saddles were used on the evaporator and condenser sections of the CPL for which these data were presented.

When using a cryogenic coolant during one of the tests, the ammonia was allowed to freeze in the condenser. In a conventional heat pipe the condenser and evaporator may be anywhere along the device. Thus, during frozen startup, the condenser may be at the longitudinal center of the heat pipe, but once vaporization and condensation begins rapid thawing occurs and the point where vapor condenses moves along the device to the normal operating position. In a CPL if there is flow blockage anywhere in the system, loop operation will be aborted. During frozen startup, a CPL must liquefy or vaporize all of the working fluid by conduction before the CPL cycle can begin.

Although the CPL can operate under large adverse tilt conditions, the device must be operating while being raised to new heights of performance. If allowed to thermally equilibrate with the surroundings at 23°C (74°F), continuous liquid contact between the evaporator and condenser will be lost at an approximate elevation of 0.254 m (10 in.). This problem can be overcome simply by increasing the initial charge pressure. However, the maximum thermal energy transport capacity would be lowered, due to increased internal pressure. Once continuous liquid contact is lost, the CPL must be primed by decreasing the system losses. For the test article, this implies lowering and cooling the evaporator section so that the liquid could rewet the wick material.

Conclusions

The CPL, when operating at a condenser temperature of 30°C, was found to be capable of continuous operation at adverse tilts of 0.61 m (24 in.). This represents a substantial wicking height when compared to conventional heat pipes. However, the device would not go through startup at an adverse tilt of more then 0.254 m (10 in.). Thus, when the final operating position requires a hydrostatic loss greater than 0.254 m, the device must be operating while increasing the adverse tilt. The effective thermal resistance was found to be relatively constant, 0.15°C/W, over much of the tested performance domain and has only a slight dependence on power input or orientation. The transport zone configuration allows the liquid and vapor to be carried over great distances with minimal pressure losses. Also, the small tubing size permits the transportation zones to be laid inside conduits and bent around corners.

Transient responses of these devices show very short reaction times and small time constants when the input power is varied. If a sudden, large demand for cooling was required, but contamination of the coolant was possible, a CPL could be used to bridge the thermal gap between a small amount of coolant in contact with the heat source and a large coolant flow that would remain untouched by contaminates. Also, a large heat flux under high acceleration could be transported quickly to a thermal sink where the energy could be dissipated gradually.

Although the computer model assumes no superheat, the predicted performance characteristics of the CPL were in good agreement with the experimental data. A model which considers a more in-depth analysis of the CPL cycle could predict the temperature profile to within ±0.5°C, and if superheated vapor were added to the model the prediction should be within ±0.1°C.

Acknowledgments

The authors wish to thank the Institute of Thermal Physics, Ural Branck of the USSR Academy of Sciences, Pervomaiskaya Str. 91, GSP-169, Sverdlovsk, 620219, USSR.

References

[1]Ku, J., and Yun, S., "A Prototype Heat Pipe Heat Exchanger for the Capillary Pumped Loop Flight Experiment," *Proceedings of the AIAA 27th Thermophysics Conference*, AIAA, Washington, DC, 1992 (AIAA Paper 92-2910).

[2]Laub, J. H., and McGinness, H. D., "Recirculation of a Two-Phase Fluid by Thermal and Capillary Pumping," California Inst. of Technology, Jet Propulsion Lab., TR 32-196, Pasadena, CA, Dec. 1961.

[3]McGinness, H. D., "Capillary Pumping for Closed-Cycle Gas Systems," California Inst. of Technology, Jet Propulsion Lab., RS 36-10, Pasadena, CA, Vol. 1, Sept. 1961, pp. 9–13.

[4]Stenger, F. J., "Experimental Feasibility Study of Water-Filled Capillary-Pumped Heat-Transfer Loops," NASA TM X-1310, Aug. 1966.

[5]Maidanik, Y., Vershinin, S., Kholodov, V., and Dolgirev, J., "Heat Transfer Apparatus," U.S. Patent 4515209, May 1985.

[6]Maidanik, Y., Fershtater, Y., and Goncharov, K., "Capillary-Pump Loop for the Systems of Thermo Regulation of Spacecraft," European Space Agency, ESA SP-324, Dec. 1991.

[7]Dunn, P., and Reay, D., *Heat Pipes*, 3rd ed., Pergamon, New York, 1982.

[8]Kaviany, M., *Principles of Heat Transfer in Porous Media*, Springer-Verlag, New York, 1991.

[9]Chapman, A., *Fundamentals of Heat Transfer*, Macmillan, New York, 1987, pp. 98–150, 159–202.

[10]Kays, W., and Crawford, M., *Convective Heat and Mass Transfer*, 3rd ed., McGraw-Hill, New York, 1993, pp. 138–140.